Synchronous fluorescence spectroscopic characterization of DMBA-TPA-induced squamous cell carcinoma in mice

Parmeswaran Diagaradjane
Mohammad A. Yaseen
Rice University
Department of Bioengineering
MS-142, P.O. Box 1892
Houston, Texas 77251

Jie Yu
Michael S. Wong
Rice University
Department of Chemical and Biomolecular Engineering
MS-362, P.O. Box 1892
Houston, Texas 77251

Bahman Anvari
Rice University
Department of Bioengineering
MS-142, P.O. Box 1892
Houston, Texas 77251
E-mail: anvari@rice.edu

Abstract. While initially confined to the epidermis, squamous cell carcinoma can eventually penetrate into the underlying tissue if not diagnosed early and treated. The noninvasive early detection of the carcinoma is important to achieve a complete treatment of the disease. Of the various non-invasive optical techniques, the synchronous fluorescence (SF) technique is considered to provide a simplified spectral profile with more sharp spectral signatures of the endogenous fluorophores in complex systems. The potential use of the SF technique in the characterization of the sequential tissue transformation in 7,12-dimethylbenz(a)anthracene–12-O-tetradecanoylphorbol-13-acetate (DMBA-TPA)-induced mouse skin tumor model in conjunction with simple statistical analysis is explored. The SF spectra show distinct differences during the earlier weeks of the tumor-induction period. Intensity ratio variables are calculated and used in three discriminant analyses. All the discriminant analyses show better classification results with accuracy greater than 80%. From the observed differences in the spectral characteristics and the ratio variables that resulted in better classification between groups, it is concluded that tryptophan, collagen, and NADH are the key fluorophores that undergo changes during tissue transformation process and hence they can be targeted as tumor markers to diagnose normal from abnormal tissues using the SF technique. © *2006 Society of Photo-Optical Instrumentation Engineers.* [DOI: 10.1117/1.2167933]

Keywords: synchronous fluorescence; cancer diagnosis; optical spectroscopy; multivariate statistics; DMBA; mouse skin carcinogenesis.

Paper 05034RR received Feb. 8, 2005; revised manuscript received Oct. 18, 2005; accepted for publication Oct. 18, 2005; published online Jan. 25, 2006.

1 Introduction

Squamous cell carcinoma, the second most common skin cancer after basal cell carcinoma, arises from the epidermis and resembles the squamous cells that comprise most of the upper layers of skin. Although squamous cell carcinomas usually remain confined to the epidermis for some time, they eventually penetrate the underlying tissues if untreated.[1] Hence, the successful treatment of the carcinoma depends on the early screening and detection. Diagnosis is often made by medical history and physical examination and confirmed by a skin biopsy. Although punch and excision biopsy techniques are considered the gold standard, they are invasive, time-consuming, and dependent on the skill of the individuals performing the procedure, and a very small portion of the suspected tissues is presented for the diagnosis.[2] Hence a noninvasive, fast, and reproducible technique for the early detection of premalignant conditions is important for successful treatment of this carcinoma.

Optical spectroscopy has been considered as an alternative technique for the conventional diagnostic methods because of its advantages, such as minimal invasiveness, less time consumption, and reproducibility.[3,4] For more than 2 decades, various optical spectroscopic techniques including fluorescence emission and diffuse reflectance have been widely explored as diagnostic tools in the discrimination of precancers and early cancers in various organ sites *in vivo*.[5] Among the various optical spectroscopic techniques, native fluorescence spectroscopy has been considered as one of the powerful techniques because of its sensitiveness to structural and microenvironmental changes of the various endogenous fluorophores present in the tissues.[6] Differences in the native fluorescence from tissues are attributed to various biomolecules such as tryptophan (Trp), tyrosine (Tyr), phenylalanine (Phe), reduced form of nicotinamide adenine dinucleotide (NADH), flavin adenine dinucleotide (FAD), collagen, elastin and endogenous porphyrins present in cells and tissues.[7] Of the various fluorophores, the fluorescence of collagen, elastin, and more generally proteins are related to the structural arrangement of cells and tissues.[8,9] The other fluorophores, pyridoxine deriva-

Address all correspondence to Bahman Anvari, Rice University, Department of Bioengineering, MS-142, P.O. Box 1892, Houston, Texas 77251. Tel.: 713–348–5870; Fax: 713–348–5877; E-mail: anvari@rice.edu

tives, NADH, FAD, and endogenous porphyrin are related to metabolic processes.[10,11] A change in the state of the tissue such as that occurring during physiological processes or in connection with the onset of pathological conditions results in modifications of the amount of fluorophores, their distribution, and the biochemical properties of their environment.[5]

Several groups have reported the use of fluorescence spectroscopy for the characterization of various types of cancers, such as those of the cervix,[12–14] oral area,[15–17] colon,[18,19] and breast.[20–22] As tissues are highly heterogeneous with many intrinsic fluorophores, fluorescence excitation/emission spectra at one and/or more excitation/emission wavelengths are used for different analytical and diagnostic applications.[5] Further, the conventional laser-induced fluorescence (LIF) spectroscopic method has limited applicability because the spectra of complex structures such as tissues often cannot be resolved satisfactorily by excitation at a single wavelength. To overcome this problem, a multiple-excitation method is used to generate an excitation-emission matrix (EEM) to identify the optimal excitation wavelengths at which tissue classification is enhanced and determine the origin of the measured fluorescence signal in a more reliable manner.[23–25] EEMs are most often used to differentiate the tissue types by selecting an emission spectra at one or a few excitation wavelengths, or excitation spectra corresponding to one or more emission wavelengths are used for the diagnostic purposes.[26–28] However, the EEM requires a series of fluorescence emission measurements at sequential excitation wavelengths at small wavelength intervals, which is a time-consuming process.

Alternatively, synchronous fluorescence (SF) spectroscopy (SFS), which is dependent on the absorption and the emission characteristics of the fluorophores can be used as a potential tool for the diagnostic purpose. The synchronous luminescence intensity is expressed as

$$I_s = KcdE_x(\lambda - \Delta\lambda)E_m(\lambda),$$

where K is a constant factor accounting for the variation in the molar extinction coefficient with respect to the intensity distribution; c is concentration of the fluorophores; d is the path length of the photons; and E_x and E_m are the intensity distribution patterns of the excitation and emission, respectively.[29] In the SFS technique, the signal is recorded by simultaneously scanning the excitation and emission wavelengths at the same speed with a fixed wavelength interval ($\Delta\lambda$) between the excitation and emission wavelengths. As indicated in the preceding equation, the wavelength of the SF spectra is the combination of both excitation and emission wavelengths and they do not represent either emission or excitation wavelengths individually. The SF spectra can be represented as a diagonal scan of the EEM with a constant wavelength different between the excitation and emission wavelengths. As the synchronous luminescence intensity involves both the excitation and emission distribution, to observe a peak, it is sufficient that either one of the two functions $E_x(\lambda - \Delta\lambda)$ or $E_m(\lambda)$ has resolved structure in the measured spectral range. Hence, SFS provides a more resolved structure from a composite system, such as tissue, in contrast to the generally featureless and broadband appearance of the conventional fluorescence spectra. Initially developed for multicomponent analysis to obtain fingerprints of

real-life samples and enhancing the selectivity in the assay of complex systems,[29–32] SFS is reported to be useful in extracting some useful information from complex biological systems.[33] Because of the characteristic sharp spectral features, SFS has been used to discriminate the normal from the abnormal conditions.[34] However, to the best of our knowledge, no reports are available on the use of *in vivo* synchronous luminescence spectra as a diagnostic tool for the discrimination of the different stages of tissue transformation during tumor progression.

The purpose of this paper is to demonstrate the potential of the SFS technique to discriminate the premalignant conditions of the skin from normal conditions, *in vivo*. As it is practically difficult to measure the spectra of a lesion in a patient, during its progression from normal to malignant condition, we used a well-established 7,12-dimethylbenz(a)anthracene–12-O-tetradecanoylphorbol-13-acetate (DMBA-TPA)-induced two-stage carcinogenesis model in mouse skin.[35] The SF spectra were measured every week (0 to 15 weeks) during the tumor induction, and analyzed using multivariate statistical techniques to demonstrate the potential of this technique in the discrimination of early stages of tissue transformation.

2 Materials and Methods

2.1 Animals

Swiss Webster female mice, 6 to 8 weeks old, were used in this study. At the beginning of the study, all animals weighed approximately 25 to 30 gm each. The animals were kept in well-ventilated polypropylene cages, and maintained in 12 h light and 12 h dark condition. The animals were fed standard laboratory diet and water *ad libitum* during the entire period of the experiments. Prior approval from the Institutional Animal Care and Use Committee at Rice University was obtained before the experiments.

2.2 Tumor Model

Healthy animals ($n=46$) were chosen and divided into two groups. Group I ($n=6$) was kept as control animals with no tumor induction and the group II ($n=40$) was used as experimental animals subjected to tumor induction process. At the beginning of the experiments, an approximately 1-cm^2 area of the hair on the dorsal side of all the animals ($n=46$) were completely removed with a clipper (blade # 40) used in conjunction with a hair removing cream (Nair). The animals were examined after 24 h for any scar formation on the skin surface. On confirmation of no scar on the skin surface, group I ($n=6$) animals were subjected to topical application of acetone only, twice weekly, for a period of 15 weeks. Tumor induction was initiated with topical application of approximately 200 μl of 0.24% of DMBA in acetone. The DMBA was applied twice weekly, over a period of 1 week. Tumor initiation was typically followed by sustained promotion with twice weekly topical application of approximately 50 to 100 μl of 5 nmol of TPA in acetone, in the same spot for 15 weeks. During the course of tumor induction, animals were monitored closely for development of papillomatous growth.
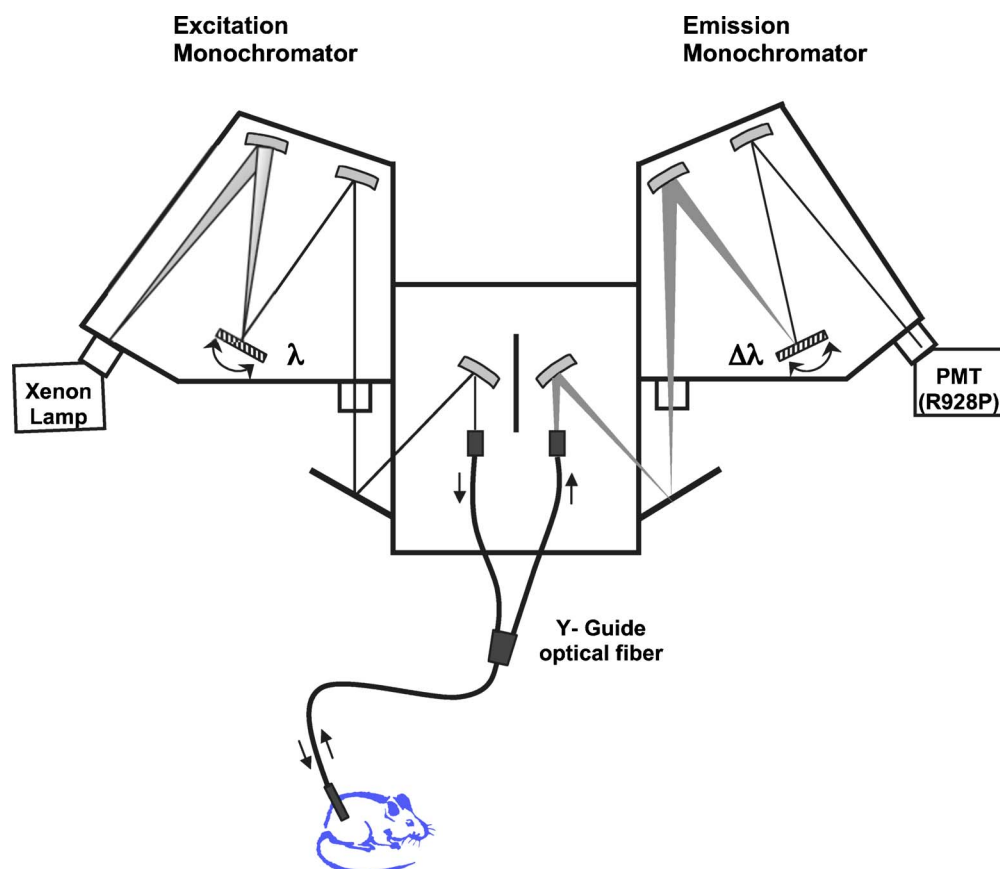
Fig. 1 Schematic of the experimental setup. The arrow in the excitation and emission monochromator represents the direction of rotation of the grating and the arrows beside the optical fiber represent the direction of excitation and emission light.

2.3 Tissues for Histological Evaluation

At different time periods (1 to 15 weeks) during the tumor induction, animals were euthanized by overdosage of isofluorane (5%). Following euthanasia, tissue specimens were excised from the tumor induction spot, using a 6-mm or 2-mm biopsy punch and preserved in 10% formalin solution for hematoxylin and eosin (H & E) staining.

2.4 SF Spectral Measurements

In vivo SF spectra were recorded using a spectrofluorometer (Fluoromax-3, ISA Jobin Yvon-Spex, Edison, New Jersey) with a Y-guide fiber optic bundle. The excitation source (150-W ozone-free xenon arc lamp), coupled to a monochromator, delivered light to a fiber optic adaptor coupled to one end of the Y-guide fiber (Fig. 1). The other end of the fiber collecting the signal was coupled to the emission monochromator connected to a photomultiplier tube (PMT; R928P, Hamamatsu, Shizuoka-Ken, Japan). During spectral measurements, the common end of the fiber probe was held perpendicular to the surface, whereas the excitation and the collection ends of the fiber assembly were connected to the excitation and emission monochromators, respectively. To ensure maximum collection of the signal over the solid angle of its origin, a spacer was used at the common end of the fiber assembly such that there was always a distance of 2 mm between the tissue surface and the fiber tip during the spectral measurements. The excitation and emission monochromator

gratings had a groove density of 1200 grooves/nm and were blazed at 330 and 500 nm, respectively. The excitation and emission slit widths were set at 3 nm each and the integration time and wavelength increment were set at 0.1 s and 1.0 nm, respectively.

During data acquisition, the excitation and the emission monochromators simultaneously collected the signals from the mouse skin with a constant wavelength difference between them and the SF signal was collected in the range 250 to 620 nm. The SF spectra from the normal mouse skin were measured at different $\Delta\lambda$ values, namely, 5, 10, 15, 20, 30, 40, and 50 nm. Among all the $\Delta\lambda$ values, $\Delta\lambda=20$ nm showed better spectral signature with good SNR and hence the value of $\Delta\lambda=20$ nm was set as the optimal value for the entire experiment. The collected signals were transferred to a PC through an RS232 interface, and processed by the Windows-based data acquisition program, DataMax (ISA Jobin Yvon-Spex, Edison, New Jersey). As the SF measurements involved the simultaneous scanning of both excitation and emission monochromators, significant contribution from the excitation light source was expected. Dividing each spectrum by the lamp spectrum measured under the same instrumental parameters minimized the contribution from the excitation light source to the SF spectra.

2.5 Statistical Analysis

The measured spectral data were analyzed statistically to discriminate the early conditions of tumor progression from nor-
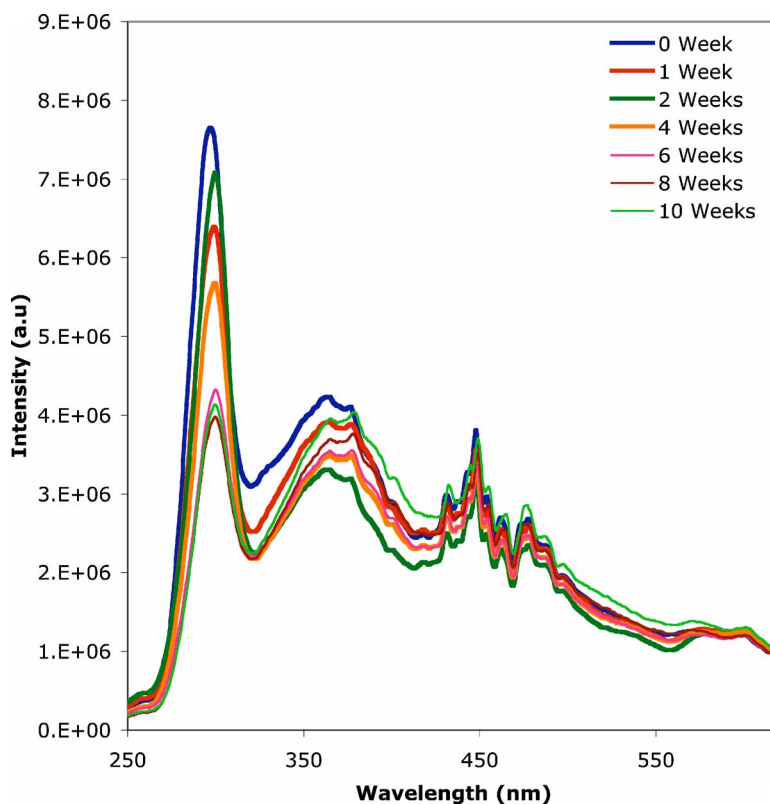
Fig. 2 Averaged SF spectra from mice skin before tumor induction (week 0) and 1, 2, 4, 6, 8, and 10 weeks after tumor induction by DMBA-TPA application.

mal condition. Data were initially preprocessed by normalizing each spectral profile with respect to its peak intensity. From each normalized spectrum, 49 SF intensity ratio variables were calculated at different wavelengths corresponding to the characteristic spectral features observed at different time periods during the tumor progression. The mean and the standard deviation values of all weeks were calculated and a two-tailed Student's t test was performed to determine the level of significance (p) of each ratio value between the control and experimental groups. Those ratio values that showed significant differences ($p < 0.001$) were selected and used as input in a discriminant analysis.

Discriminant analysis was performed for three categories based on the tumor progression. Immediately after the tumor initiation by DMBA, inflammatory response against the applied carcinogen is initiated leading to morphological changes. To discriminate the immediate changes after the tumor initiation, discriminant analysis 1 was performed between normal and 1 week after DMBA application. The rationale for discriminant analysis 2 was based on the fact that the application of DMBA (initiator) increases the probability of initiation for a short while, but does not change the mitotic and death rates of any of the cell types. The initiated cells will remain in the latent stage until a suitable promoter agent is applied. The subsequent application of TPA (promoter) was expected to produce changes in the mitotic and death rates of the cells. Hence, these analyses were performed across three data sets corresponding to the SF measurements before DMBA application (week 0), after DMBA application (week 1) and each week after TPA application (weeks 2 to 15). As

the tissue morphological changes during the tumor induction will be different for each animal, the discriminant analysis 3 was performed by grouping the data sets based on the histological findings. The data sets were grouped anticipating that inflammatory and hyperplastic conditions appear during the first week, dysplastic conditions between the second and fifth weeks, moderately differentiated invasive squamous cell carcinoma during weeks 6 to 10, and poorly differentiated squamous carcinoma between 11 and 15 weeks.

Stepwise multiple/linear discriminant analyses were performed using SPSS/PC+ 8.0 statistical software. The discriminant analyses used a partial F test and a stepwise method to sequentially incorporate the set of 49 variables into a Fisher linear discriminant function. In stepwise discriminant function analysis, a model of discrimination is built step by step. Specifically, at each step, all variables are reviewed and evaluated to determine which one will contribute most to the discrimination between groups. Stepwise discriminant analysis performed among n groups would generally result in the coefficients of n Fisher linear discriminant (or) classification functions (one for each group) and $(n-1)$ canonical discriminant functions. The classification function of each group (original grouped cases) discriminates only that group from the rest of the groups in the analysis.[36–41] To check the reliability of our analysis, leave-one-out cross-validation was used.[41,42] In this procedure, discriminant scores of one particular case were eliminated and discriminant analysis was used to form a classification algorithm using the remaining samples. The resulting algorithm was then used to classify the
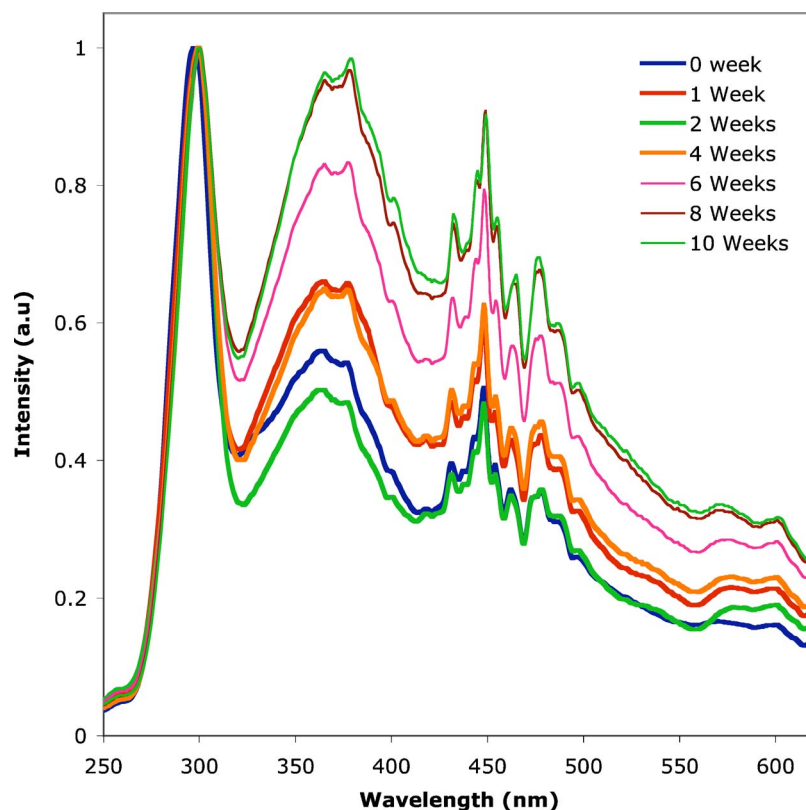
Fig. 3 Averaged normalized SF spectra from mouse skin before tumor induction (week 0) and 1, 2, 4, 6, 8, and 10 weeks after tumor induction by DMBA-TPA application.

excluded case. This process was repeated for each of the cases (cross-validated grouped cases). This process provides optimal use of a small data set to validate the performance of a decision without bias. The proportion of the classification showing true negative and true positive results were used to estimate the specificity and sensitivity. The overall classification accuracy was determined from the entire data set correctly classified in to the respective groups.

3 Results

3.1 SF Characteristics of Mouse Skin

The SF spectra of skin from different animals were averaged at every week and compared with the normal mouse skin for differences in spectral signature. A representative averaged spectra at 0, 1, 2, 4, 6, 8, and 10 weeks is shown in Fig. 2. The average SF spectrum before the application of DMBA-TPA shows a prominent peak at 299 nm and two secondary peaks around 368 and 450 nm. The primary peak observed at 299 nm may be attributed to the aromatic amino acid residues such as tyrosine and tryptophan, whereas the secondary peaks around 368 and 450 nm may be attributed to the structural proteins and coenzymes respectively.[34] After tumor initiation and promotion by DMBA-TPA, the prominent 299-nm peak in the case of normal mouse skin was shifted to 302 nm in the case of experimental groups. However, no significant changes were observed in the position of the secondary peaks in the case of experimental animals when compared to that before DMBA application. The spectral intensity of these peaks decreased in the experimental group of animals 1 week after the

tumor induction by DMBA-TPA. In the case of experimental groups, after the DMBA-TPA application, two additional broad peaks centered at 540 nm and in the range of 570 to 610 nm were also observed. These additional peaks may be attributed to FAD and porphyrins respectively.

The spectral profiles at the subsequent weeks showed similar features, except for the differences in the intensity values at the characteristic wavelengths of the different fluorophores. The spectral intensity at 302 nm was maximum in the second week, gradually decreased with increasing weeks of tumor induction, and remained almost the same after the eighth week onward. However, the intensity of the secondary peak centered at 368 nm decreased gradually until the sixth week after tumor induction and slowly increased from 6 weeks onward. It was also observed that the bandwidth of the secondary peak increased after the sixth week, indicating the increasing contribution from a different fluorophore in this spectral region. The spectral profile of the control group (acetone only) did not show any significant changes with increasing weeks of acetone application.

To understand the relative contribution of the different fluorophores, each spectrum was normalized with respect to its maximum peak intensity value. While the process of normalization eliminates the absolute intensity information, the main advantage of using normalized spectrum is that the intensity need not be recorded in calibrated units.[13] The normalized average synchronous fluorescence (SF) spectra of the experimental groups of animals at week 0 and 1, 2, 4, 6, 8, and 10 weeks after DMBA-TPA application is shown in Fig. 3.
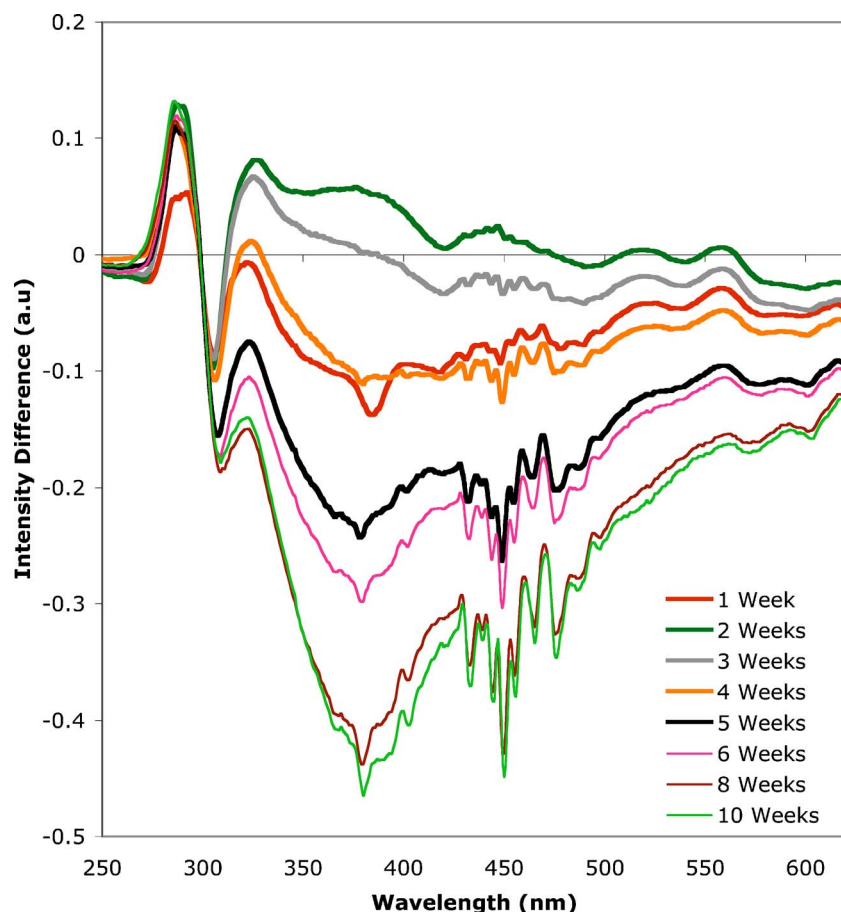
Fig. 4 Difference spectra between the normalized SF at week 0 and 1, 2, 3, 4, 5, 6, 8, and 10 weeks after DMBA-TPA application.

The difference spectra between week 0 and 1, 2, 3, 4, 5, 6, 8, and 10 weeks after the tumor induction is shown in Fig. 4. Distinct spectral differences were observed in the case of experimental groups during the earlier weeks (weeks 1 to 4) of tumor induction. However, no significant differences were found in the spectral profiles of the experimental groups after 10 weeks (data not shown).

3.2 *SFS of Standard Fluorophores*

To confirm the origin of the observed spectral peaks and assign them to various endogenous fluorophores, the SF spectra of commercial grade fluorophores (Sigma Chemicals, USA) phenylalanine, tyrosine, tryptophan, collagen, elastin, nicotinamide adenine dinucleotide (NAD), NADH, FAD, and protoporphyrinIX (ppIX) were measured under the same experimental conditions as for the mouse skin. The SFS of the commercial grade fluorophores were corrected for the variation in the lamp intensity and normalized with respect to the corresponding peak intensity. The normalized SF spectra of the aromatic amino acids (phenylalanine, tyrosine, tryptophan), structural proteins (collagen, elastin), coenzymes (NAD, NADH), FAD and ppIX are shown in Figs. 5(a) to 5(d) respectively. The dominant peaks for phenylalanine, tyrosine, tryptophan, collagen, elastin, NAD, NADH, FAD and ppIX were observed at 277, 288, 309, 365, 379, 380, 403, 570, and 405 nm respectively. The SFS of tyrosine, elastin, and FAD also showed secondary peaks around 355, 436, and

370 nm, respectively. In addition to the secondary peak at 436 nm [Fig. 5(b)] sharp spectral features were observed at 467 nm, which are attributed to the contribution from the xenon lamp source. As the xenon lamp has the characteristic spectral peak that is more specific at 467 nm, the small secondary shoulder observed around 436 nm is attributed to the elastin. The SF spectra of ppIX showed additional peaks at 530, 562, and 606 nm.

3.3 *Multivariate Statistical Analysis*

3.3.1 *Discriminant analysis 1*

The stepwise linear discriminant analysis was performed between the data set before DMBA application (week 0) and the experimental group after DMBA application (week 1) to identify the SF intensity ratio variables, which can detect the immediate changes in the mouse skin, induced by DMBA application. In this analysis, out of the 49 input variables, only 3 variables turned out to be the most significant and were included in the linear discriminant analysis, which resulted in the following discriminant function (Df_1):

$$Df_1 = 7.47(I_{320}/I_{375}) - 17.61(I_{365}/I_{420}) + 25.68(I_{540}/I_{560})$$
$$- 5.10,$$

where the values I represents the SF intensity values corresponding to the wavelengths given in the subscripts.
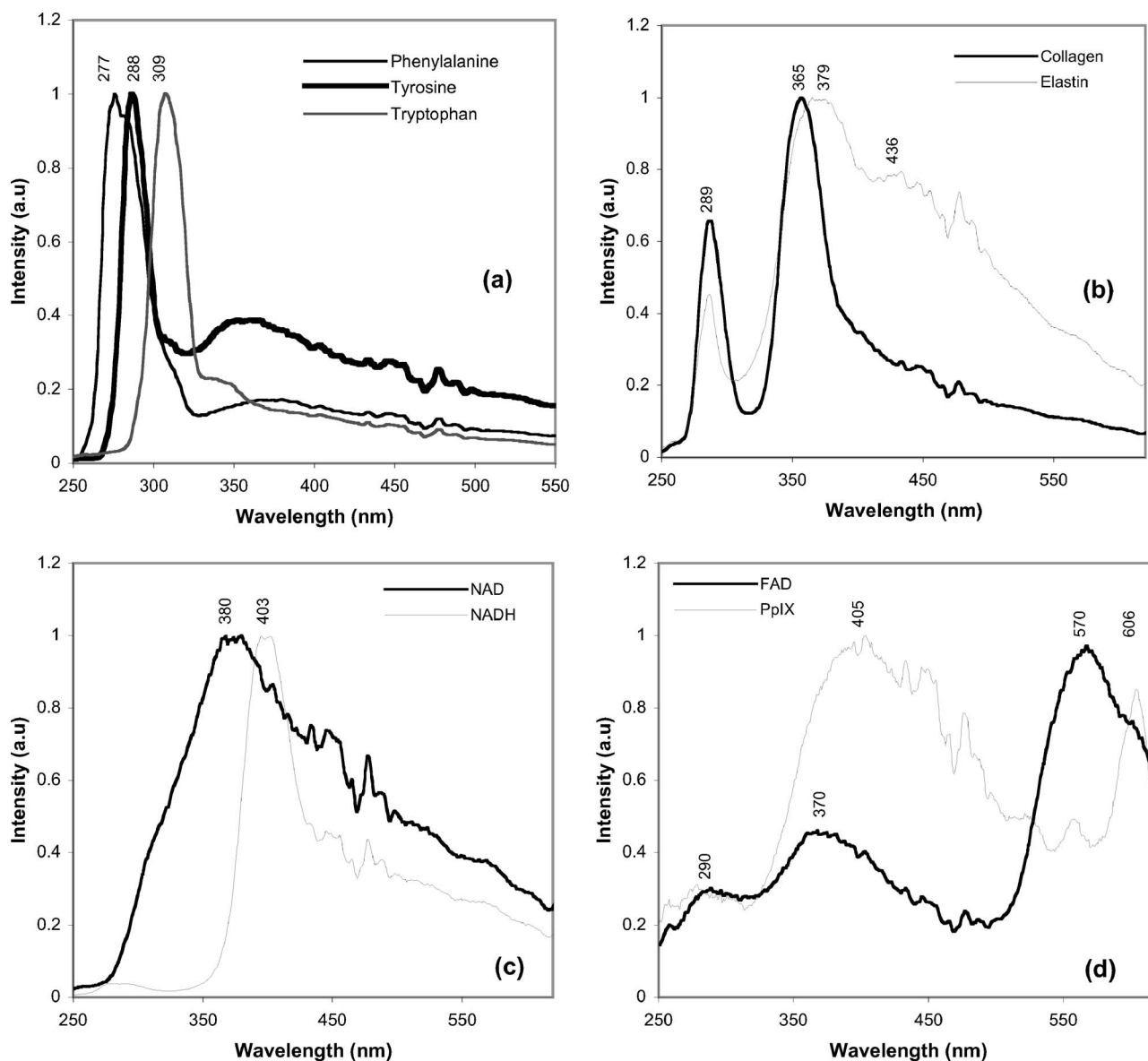
Fig. 5 Normalized SF spectra of the standard fluorophores (a) phenylalanine, tyrosine, and tryptophan, (b) collagen and elastin, (c) NAD and NADH, and (d) FAD and ppIX.

This discriminant function classified the original grouped cases with a specificity and sensitivity of 100 and 92.5%, respectively, and the cross-validated grouped cases with a specificity and sensitivity of 97.8 and 92.5%, respectively. The overall classification accuracy for the original grouped cases and cross-validated grouped cases was 96.5 and 95.3%, respectively. The scatter plot of Df_1 for 0 and 1 week groups of animals and the associated error bars are shown in Fig. 6.

3.3.2 Discriminant analysis 2

The stepwise multiple linear discriminant analyses performed across the various groups and their classification results are summarized in Table 1. From Table 1, we observe that the discriminant analysis between weeks 0, 1, and 6 showed better discrimination with a specificity of 100% and sensitivities of 95 and 100% for the weeks 1 and 6, respectively, for the original grouped cases. The cross-validated grouped cases

showed a specificity of 97.8% and sensitivities of 92.5 and 100%, respectively. The overall accuracy of the original data and the cross-validated data is observed as 98.3 and 97.4%, respectively. The overall accuracy of the discriminant analyses performed across the other group categories showed relatively less classification accuracy when compared to that across the groups, for weeks 0, 1, and 6. Nine statistically significant intensity ratio variables formed the discriminant functions Df_2 and Df_3 to discriminate the 0-, 1-, and 6-weeks group of animals. The scatter plot of Df_2 versus Df_3 for the groups for weeks 0, 1, and 6 is shown in Fig. 7, along with the group centroids and the error bars.

3.3.3 Discriminant analysis 3

The data set were grouped as (1) group I, before DMBA application; (2) group II, 1 week after DMBA application; (3) group III, 2 to 5 weeks after DMBA-TPA application; (4)
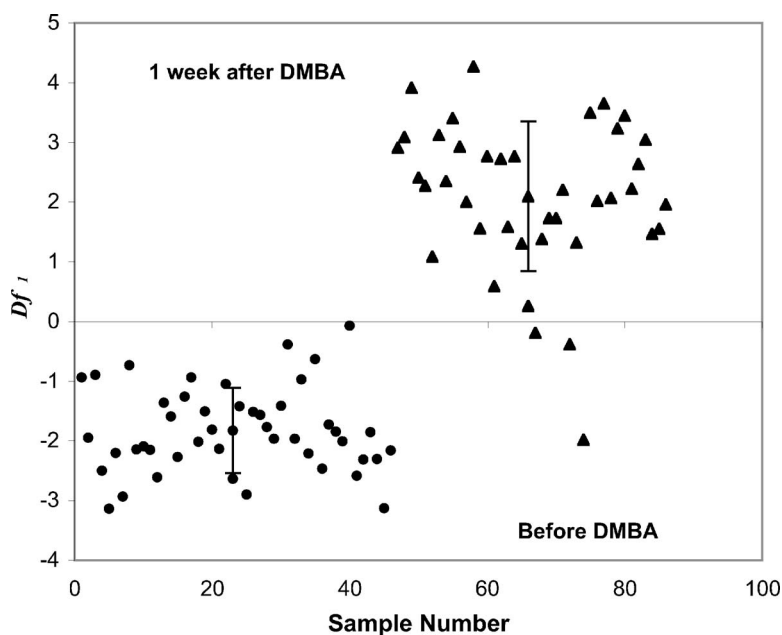
Fig. 6 Scatter plot showing the distribution of Df_1, from the discriminant analysis 1, for normal mouse skin before DMBA application (week 0) and one week after DMBA application.

group IV, 6 to 10 weeks after DMBA-TPA application; and (5) group V, 11 to 15 weeks after DMBA application. A stepwise discriminant analysis was performed across these five groups. The classification results of this discriminant analysis are summarized in Table 2. The percentage classification of the original grouped data and the cross-validated grouped data is observed as 87.4 and 85.4%, respectively. Sixteen statistically significant intensity ratio variables formed the discriminant functions Df_4, Df_5, Df_6, and Df_7 to discriminate the five groups. The scatter plot of Df_4 versus Df_5 versus Df_6 for the five groups is shown in Fig. 8.

4 Discussion

Several endogenous fluorophores in tissues were identified and the changes in concentration and conformation of these fluorophores during the onset of pathological conditions were exploited for discrimination of normal from premalignant and malignant conditions at different organ sites.[2–6,43] In this study, the diagnostic potential of SFS was explored to discriminate the various stages of tissue transformation in DMBA-TPA-induced squamous cell carcinoma in mouse skin. The spectral data were analyzed using multivariate statistical methods to determine the accuracy of classification between normal and abnormal conditions.

SF spectra are considered to provide a simple and rapid way to measure the spectral fingerprints of complex biological samples. It has been reported that the SFS of single molecular species presents a narrower spectral band than the conventional fluorescence spectrum.[29,31] The utility of SFS in identifying the different components in a complex mixture has been reported and the technique is capable of providing distinct spectral signatures with high resolution of the chemicals that are similar in chemical structure.[33] The major advantage of the SF technique is that all the biological components in complex structures like tissues are excited under optimal condi-

tions (wavelength of excitation, the slit widths, scan speed, scan range), which is practically impossible in the case of conventional fluorescence measurements. In the case of conventional fluorescence measurements, the optimal conditions are chosen based on the fluorophore(s) of interest. Further, the synchronous fluorescence spectrum represents the diagonal scan over the entire EEM, thereby reducing the time of data acquisition without any alterations in the details over the entire spectral range of the different fluorophores present in the tissues.

The comparison of mouse skin SF spectra with those corresponding to commercial fluorophores suggests that the peaks observed at 300, 370, 450, 535, and 600 nm in the spectra of mouse skin may be attributed to the tyrosine and tryptophan residues, structural proteins collagen and elastin, NADH, and porphyrins. Similar SF spectral peaks from the endogenous fluorophores were reported earlier in the discrimination of normal tissues from oral cancer tissues.[34] Further, the fine structures observed in the wavelength range between 440 and 500 nm may be due to the stray light contribution from the xenon lamp passing through the exit slit of the excitation monochromator. In this study, the wavelengths of the spectral peaks observed in the case of mouse skin were not exactly the same as those of the standard fluorophores. This observed spectral shift of the peak positions in the spectra of mouse skin may be due to the different microenvironments of these endogenous fluorophores in tissues. The spectral peak intensity observed at 299 nm for the normal mouse skin is red shifted to 302 nm, after the tumor initiation by DMBA. Similar spectral peak shifts were reported on the SF spectra of normal and neoplastic cells *in vitro*.[32]

The variations in the spectral intensity observed through the sixth week may be due to the epithelial thickening, redness, and other morphological changes induced by the

Table 1 Classification results of discriminant analysis 2.

Groups	Weeks	Original Data[a] (%)			Cross-Validated Data[b] (%)		
		Specificity	Sensitivity	Overall Accuracy	Specificity	Sensitivity	Overall Accuracy
1	0	97.8	—		97.8	—	
	1	—	77.5	82.4	—	77.5	82.4
	2	—	69.2		—	69.2	
2	0	97.8	—		95.7	—	
	1	—	85.0	92.7	—	85.0	91.1
	3	—	94.6		—	91.9	
3	0	97.8	—		95.7	—	
	1	—	90.0	95.9	—	87.5	94.3
	4	—	100		—	100	
4	0	97.8	—		95.7	—	
	1	—	95.0	97.5	—	92.5	95.8
	5	—	100		—	100	
5	0	97.8	—		97.8	—	
	1	—	95.0	97.5	—	92.5	96.6
	6	—	100		—	100	
6	0	100	—		100	—	
	1	—	95.0	98.3	—	92.5	97.4
	7	—	100		—	100	
7	0	97.8	—		97.8	—	
	1	—	92.5	96.5	—	92.5	96.5
	8	—	100		—	100	
8	0	97.8	—		97.8	—	
	1	—	92.5	96.5	—	92.5	96.5
	9	—	100		—	100	
9	0	97.8	—		97.8	—	
	1	—	92.5	96.4	—	92.5	96.4
	10	—	100		—	100	
10	0	97.8	—		97.8	—	
	1	—	92.5	96.4	—	92.5	96.4
	11	—	100		—	100	
11	0	97.8	—		97.8	—	
	1	—	92.5	96.4	—	92.5	96.4
	12	—	100		—	100	
12	0	97.8	—		97.8	—	
	1	—	92.5	96.4	—	92.5	96.4
	13	—	100		—	100	
13	0	100	—		97.8	—	
	1	—	95.0	98.2	—	92.5	96.4
	14	—	100		—	100	
14	0	100	—		97.8	—	
	1	—	95.0	98.2	—	92.5	96.4
	15	—	100		—	100	

[a]Classification between the grouped original data (groups 1 through 14).
[b]Cross-validation is done only for those cases included in the original analysis. In cross-validation, each case is classified by a function derived from all cases, other than that case.
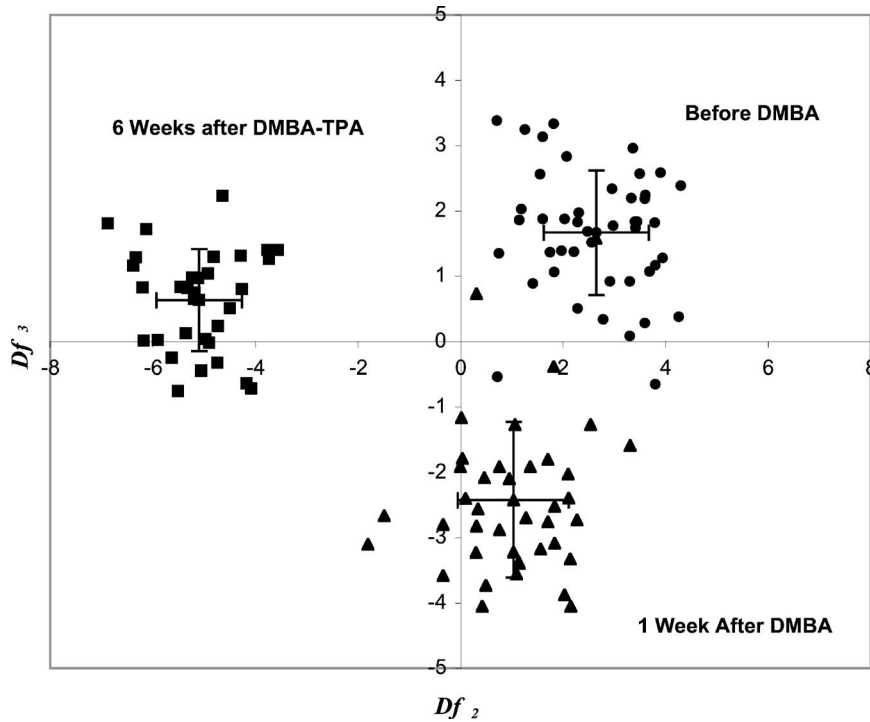
Fig. 7 Scatter plot showing the distribution of Df_2 versus Df_3, from the discriminant analysis 2, for normal mouse skin before DMBA application (week 0), one week after DMBA application, and six weeks after DMBA/TPA application.

DMBA-TPA application. In particular, the epithelial thickening may alter the tissue optical properties, leading to the reabsorption of the emission from the fluorophores resulting in less spectral intensity. The redness of the tissues due to the increased blood pigmentation may also lead to reabsorption of the emission by hemoglobin. After the sixth week, the spectral peak at 370 nm was broadened, which may be attributed to

Table 2 Classification results of discriminant analysis 3.

| Data Set | Groups | Predicted Group Membership (%) | | | | | Overall Accuracy |
		I	II	III	IV	V	(%)
Original[a]	I	**93.5**	2.2	4.3	0.0	0.0	
	II	5.0	**85.0**	10.0	0.0	0.0	
	III	2.1	3.4	**93.2**	1.4	0.0	87.4
	IV	0.0	0.0	6.9	**75.9**	17.2	
	V	0.0	0.0	0.0	7.3	**92.7**	
Cross-validated[b]	I	**93.5**	2.2	4.3	0.0	0.0	
	II	5.0	**80.0**	15.0	0.0	0.0	
	III	2.1	4.8	**91.8**	1.4	0.0	85.4
	IV	0.0	0.0	8.3	**73.8**	17.9	
	V	0.0	0.0	0.0	9.7	**90.3**	

The numbers in the bold represents the percentage of cases classified correctly in that group.
[a]Classification between the grouped original data (group I, week 0; group II, week 1; group III, weeks 2 to 5; group IV, weeks 6 to 10; group V, weeks 10 to 15).
[b]Cross-validation is done only for those cases included in the original analysis. In cross-validation, each case is classified by a function derived from all cases, other than that case.
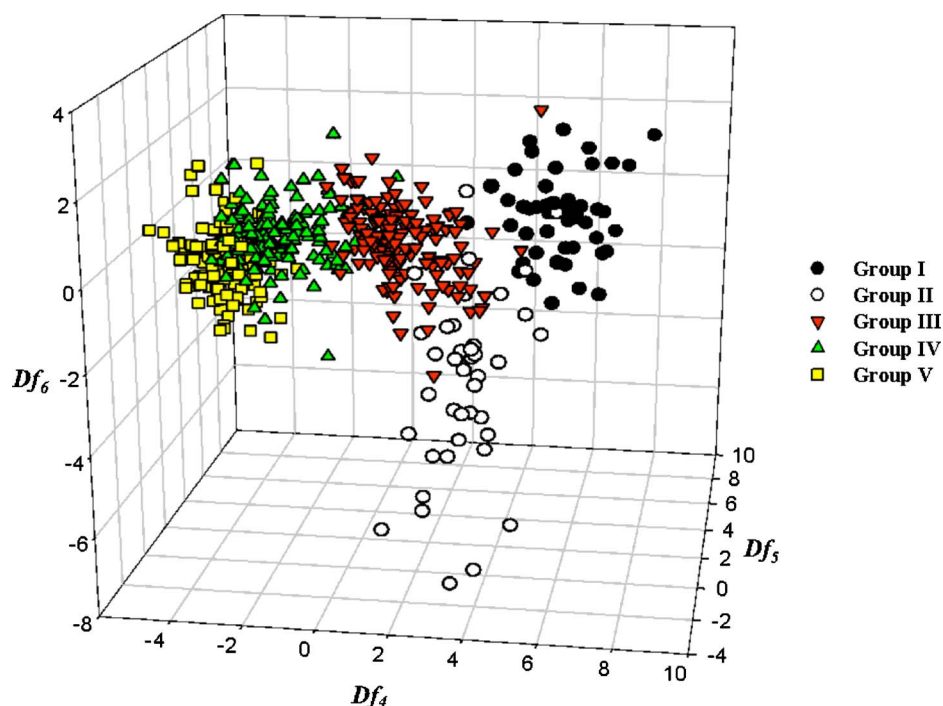
Fig. 8 Scatter plot showing the distribution of Df_4 versus Df_5 versus Df_6 from the discriminant analysis 3, for group I (no DMBA application, week 0), group II (one week after DMBA application), group III (2 to 5 weeks after DMBA-TPA application), group IV (6 to 10 weeks after DMBA-TPA application), and group V (11 to 15 weeks after DMBA-TPA application).
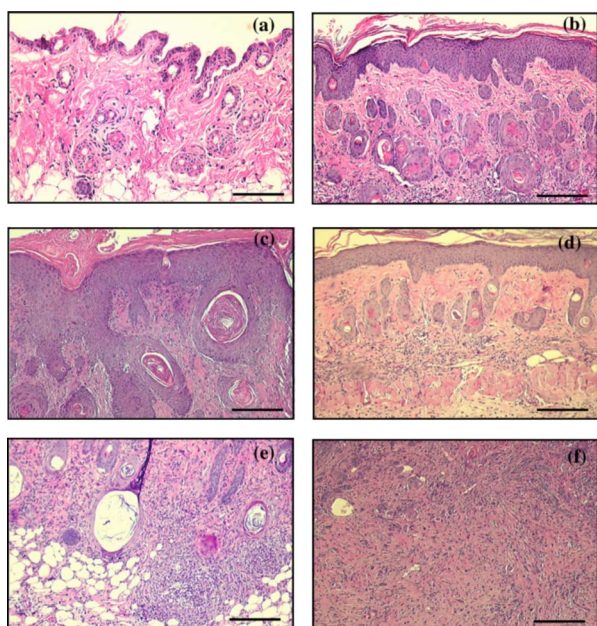
Fig. 9 H&E stained section of mouse skin before and after DMBA-TPA application (a) normal mouse skin without any DMBA application, (b) hyperplastic changes in the first week after DMBA application alone, (c) dysplastic changes and keratin pearl formation in the fifth week, (d) hyperplastic changes and inflammatory response in the second week, (e) moderately differentiated invasive squamous cell carcinoma in the third week (typical representation of the earliest occurrence), and (f) very advanced poorly differentiated invasive squamous cell carcinoma in the 15th week after DMBA-TPA application.

increased contribution of NADH. These observations correlate with the earlier reports on the influence of epithelial thickening on skin autofluorescence[44] and the increased level of NADH in the premalignant and malignant tissues than in the normal tissues.[30,45,46] The broad and relatively less intense spectral peak at 600 nm, observed from the first week of DMBA application, may be attributed to the endogenous porphyrins present in the tissues because premalignant tissues tend to accumulate endogenous porphyrins, which are the end products of the heam-biosynthesis pathway.[47,48] However, the existence of the porphyrin peak was not appreciably noticeable in the averaged spectra and also in the normalized average spectra of the experimental groups. This was because all the animals did not undergo the same tissue transformation process.

To confirm the different morphological changes that occur during tissue transformation process, animals were sacrificed randomly for histological evaluation. Histological images of the mouse skin at different time periods are shown in Figs. 9(a) to 9(f). During the earlier weeks (weeks 2 to 6) of tumor induction, most of the tissues showed dysplastic changes. However, some tissues displayed moderately differentiated invasive squamous cell carcinoma, which is widely seen in the tissue biopsies between 6 and 10 weeks. In 15 weeks, complete development of the tumor was observed with numerous cells and histologically categorized as poorly differentiated invasive squamous cell carcinoma. The SFS corresponding to the histology slides mentioned in Figs. 9(a) to 9(e) are shown in Figs. 10(a) to 10(e). Depending on the morphological conditions the individual SF spectra showed prominent peaks. In particular, the SF spectra corresponding to 1 week after
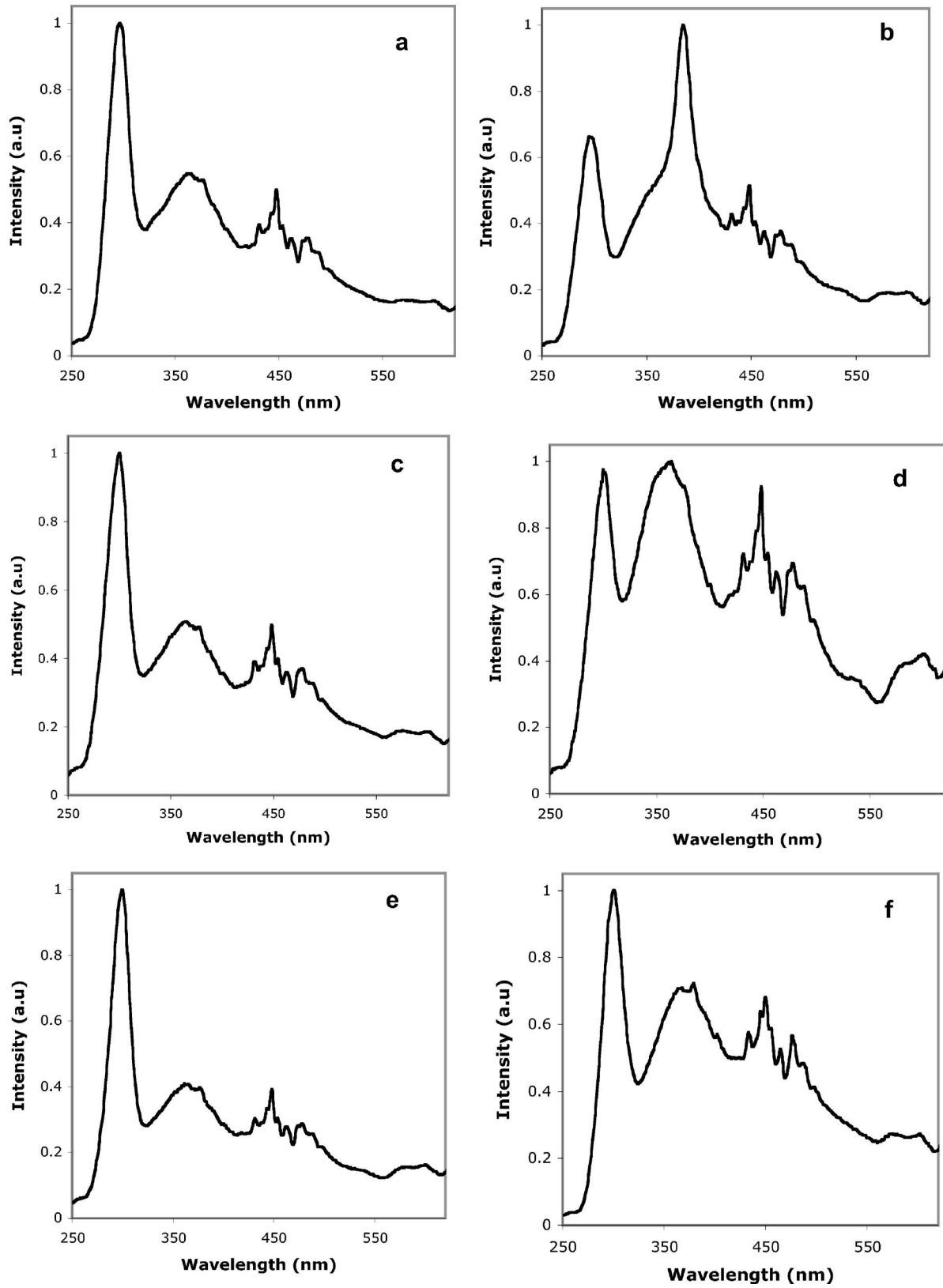
Fig. 10 Normalized SF spectra of the mouse skin corresponding to the histology sections shown in Figs. 9(a)–9(f).

DMBA application [Fig. 10(b)] showed a sharp peak at 386 nm that may be attributed to the NADH, which is usually enhanced in highly metabolic conditions. After initiation with the DMBA, the inflammatory response was triggered in the skin, thereby increasing the metabolic activity of the cells, leading to increased level of NADH. Further, it is also observed that the porphyrin peaks are enhanced in all the cases except for the normal mouse skin, indicating the definite morphological changes induced by the DMBA-TPA application.

Although significant spectral differences were observed between the normal skin and that at different weeks of the tumor induction process, a definitive quantitative method is required for the classification purpose. Hence, a simple statistical method was adopted based on the ratio values estimated from the intensities at different wavelengths characterizing the peaks and valleys of different groups under study.

Discriminant analysis 1 resulted in a discriminant function involving only three ratio variables, I_{320}/I_{375}, I_{365}/I_{420}, and I_{540}/I_{560}, indicating that the fluorophores, collagen, elastin, NADH, and flavin, corresponding to these wavelengths are responsible for the better discrimination of the normal group from the experimental group at 1 week after DMBA application. Note that the presence of 420 nm in the contributing ratio variables indicates that there is significant variation in the hemoglobin reabsorption before and after DMBA application. The DMBA application induces changes in the vasculature, leading to the differences in the hemoglobin absorption at 420 nm, at different stages of tissue transformation.

Discriminant analysis 2 showed better classification results in the sixth week. In group I (0, 1, and 2 weeks), the specificity and sensitivities were observed as 97.8, 77.5, and 69.2%, respectively. The sensitivity values were less because of the strong overlap of the spectral profiles in the first- and second-week groups. However, with increasing weeks, the specificity and sensitivity values increased gradually up to sixth week and then it decreased slowly and remained almost the same for all the weeks in the later stages of tumor induction (Table 1). From the ratio values, it is observed that the contribution of the peak emission intensity from tryptophan, collagen, and NADH and their relative distribution with respect to the other plays a significant role in the discrimination of the experimental group at 6 weeks with respect to normal and the first week.

To have a simple and broad classification, the data sets were grouped as (1) group I, before DMBA application; (2) group II, 1 week after DMBA application; (3) group III, 2 to 5 weeks after DMBA-TPA application; (4) group IV, 6 to 10 weeks after DMBA-TPA application; and (5) group V, 11 to 15 weeks after DMBA-TPA application. The data sets were grouped based on the earlier reports on the different stages of tissue transformation in DMBA induced carcinogenesis (chronic application) in hamster cheek pouch.[49] The chronic application of DMBA pushes the epithelial lining of the cheek pouch through the stages of inflammation, hyperplasia, dysplasia, and both benign and malignant tumor formation.[27] As the presented mouse skin tumor model is similar to the hamster cheek pouch model, the data sets were grouped as just mentioned. As in discriminant analysis 1 and discriminant analysis 2, 49 ratio variables were used, out of which 17 variables were found to be significant in the best classification of the five groups with respect to each other. The overall classification accuracy for the original and cross-validated data was 87.4 and 85.4%, respectively. However, in both the original data and the cross-validated data the specificity is found to be 93.5%, indicating that there exists a clear distinction between the normal mouse skin and the DMBA-TPA-induced mouse skin. From the classification results (Table 2), it is observed that group IV and group V are misclassified, as the other indicating that during the later weeks of tumor induction, the classification accuracy is slightly decreased. However, note that none of the cases in either group IV or group V were misclassified as normal. These results correlate well with the results of discriminant analysis 2, where the group 6, corresponding to the sixth week is better classified than the other groups.

The results of this study suggest that the SFS in conjunction with a simple statistical analysis has the potential for diagnosis of premalignant and malignant conditions from the normal tissues. The spectral signatures and the statistical results suggest that tryptophan, collagen, and NADH are the key endogenous fluorophores that can be used as tumor markers to diagnose the tissue transformation process. In spite of these key fluorophores, significant contributions from endogenous porphyrin are also observed with the tissue morphological changes. However, to categorically diagnose the different tissue morphological changes such as hyperplasia, dysplasia, carcinoma *in situ*, well-differentiated squamous cell carcinoma, moderately differentiated squamous cell carcinoma, and poorly differentiated squamous cell carcinoma, studies are required with larger numbers of animals, and the spectral profiles of each histological category should be grouped for the classification statistics. Further, extensive studies on tissue biopsies from human subjects under different pathological conditions are necessary to optimize the parameters for the SFS before using it for real-time *in vivo* clinical diagnosis of cancer.

References

1. Website: http://www.skincancer.org.
2. G. Zonios, L. T. Perelman, V. Backman, R. Manoharan, M. Fitzmaurice, J. Van Dam, and M. S. Feld, "Diffuse reflectance spectroscopy of human adenomatous colon polyps in vivo," *Appl. Opt.* **38**, 6628–6637 (1999).
3. R. R. Alfano, D. B. Tata, J. Cordero, P. Tomashefsky, F. W. Longo, and M. A. Alfano, "Laser induced fluorescence spectroscopy from native cancerous and normal tissue," *IEEE J. Quantum Electron.* **QE-20**, 1507–1511 (1984).
4. S. Andersson-Engels, J. Johansson, K. Svanberg, and S. Svanberg, "Fluorescence imaging and point measurements of tissue: application to demarcation of malignant tumors and atherosclerotic lesions from normal tissue," *Photochem. Photobiol.* **53**, 807–814 (1990).
5. R. Richards-Kortum and E. Sevick-Muraca, "Quantitative optical spectroscopy for tissue diagnosis," *Annu. Rev. Phys. Chem.* **47**, 555–606 (1996).
6. N. Ramanujam, "Fluorescence spectroscopy in vivo," in *Encyclopedia of Analytical Chemistry*, R. A. Meyers, Ed., pp. 20–56, John

Wiley & Sons, Chichester (2000).

7. C. R. Kapadia, W. F. Cutruzzola, K. M. O'Brien, M. L. Stetz, R. Enriquez, and L. I. Deckelbaum, "Laser induced fluorescence spectroscopy of human colonic mucosa," *Gastroenterology* **99**, 150–157 (1990).

8. R. R. Alfano, G. C. Tang, A. Pradhan, W. Lam, D. S. J. Choy, and E. Opher, "Fluorescence spectra from cancerous and normal human breast and lung tissues," *IEEE J. Quantum Electron.* **QE-23**, 1806–1811 (1987).

9. N. Ramanujam, "Fluorescence spectroscopy of neoplastic and non-neoplastic tissues," *Neoplasia* **1–2**, 89–117 (2000).

10. M. Monici, R. Pratesi, P. A. Bernabei, R. Caporale, P. R. Ferrini, A. C. Croce, P. Balzarini, and G. Bottiroli, "Natural fluorescence of white blood cells: spectroscopic and imaging study," *J. Photochem. Photobiol., B* **30**, 29–37 (1995).

11. B. Chance, I. A. Salkovitz, and A. G. Kovach, "Kinetics of mitochondrial flavoprotein and pyridine nucleotide in perfused heart," *Am. J. Physiol.* **1**, 207–218 (1972).

12. A. Mahadevan, M. Follen, E. Silva, S. Thomsen, and R. Richards-Kortum, "Study of the fluorescence properties of normal and neoplastic human cervical tissue," *Lasers Surg. Med.* **13**, 647–655 (1993).

13. N. Ramanujam, M. Follen-Mitchell, A. Mahadevan-Jansen, S. Thomsen, G. Staerkel, A. Malpica, T. Wright, N. Atkinson, and R. Richards-Kortum, "Cervical precancer detection using multivariate statistical algorithm based on laser-induced fluorescence spectra at multiple excitation wavelengths," *Photochem. Photobiol.* **64**, 720–735 (1996).

14. A. Agarwal, U. Utzinger, C. Brookner, C. Pitris, M. F. Mitchell, and R. Richards-Kortum, "Fluorescence spectroscopy of the cervix: influence of acetic acid, cervical mucus, and vaginal medications," *Lasers Surg. Med.* **25**, 237–249 (1999).

15. D. R. Ingrams, J. K. Dhingra, K. Roy, D. F. Perrault Jr., I. D. Bottrill, S. Kabani, E. E. Rebeiz, M. M. Pankratov, S. M. Shapshay, R. Manoharan, I. Itzkan, and M. S. Feld, "Autofluorescence characteristics of oral mucosa," *Head Neck* **19**, 27–32 (1997).

16. V. Kolli, H. E. Savage, T. J. Yao, and S. P. Schantz, "Native cellular fluorescence of neoplastic upper aerodigestive mucosa," *Arch. Otolaryngol. Head Neck Surg.* **121**, 1287–1292 (1995).

17. S. P. Sschantz, V. Kolli, H. E. Savage, G. Yu, J. P. Shah, D. E. Harris, A. Katz, R. R. Alfano, and A. G. Huvos, "In vivo native cellular fluorescence and histological characteristics of head and neck cancer," *Clin. Cancer Res.* **4**, 1177–1182 (1998).

18. K. T. Schomaker, J. K. Frisoli, C. C. Compton, T. J. Flotte, J. M. Richter, N. S. Nishioka, and T. F. Deutsch, "Ultraviolet laser-induced fluorescence of colonic tissue: basic biology and diagnostic potential," *Lasers Surg. Med.* **12**, 63–78 (1992).

19. M. A. Mycek, K. T. Schomacker, and N. S. Nishioka, "Colonic polyp differentiation using time-resolved autofluorescence spectroscopy," *Gastrointest Endosc* **48**, 390–394 (1998).

20. R. R. Alfano, G. C. Tang, A. Pradhan, W. Lam, D. S. J. Choy, and E. Opher, "Fluorescence spectra from cancerous and normal human breast and lung tissues," *IEEE J. Quantum Electron.* **QE-23**, 1806–1811 (1987).

21. S. Nioka, M. Miwa, S. Orel, M. Shnall, M. Haida, S. Zhao, and B. Chance, "Optical imaging of human breast cancer," *Adv. Exp. Med. Biol.* **361**, 171–179 (1994).

22. G. M. Palmer and N. Ramanujam, "Diagnosis of breast cancer using optical spectroscopy," *Med. Laser Appl.* **18**, 233–248 (2003).

23. R. A. Zangaro, L. Silveira, R. Manoharan, G. Zonios, I. Itzkab, R. Dasari, J. C. Van Dam, and M. S. Feld, "Rapid multiexcitation fluorescence spectroscopy system for in vivo tissue diagnosis," *Appl. Opt.* **35**, 5211–5219 (1996).

24. A. Zuluga, U. Uitzinger, A. Durkin, H. Fuchs, A. Gillenwater, R. Jacob, B. Kemp, L. Fan, and R. Richards-Kortum, "Fluorescence EEMs of human tissue: a system for in vivo measurements and method of data analysis," *Appl. Spectrosc.* **53**, 302–310 (1999).

25. G. M. Palmer, C. Zu, T. M. Breslin, F. Xu, K. W. Gilchrist, and N. Ramanujam, "Comparison of multiexcitation fluorescence and diffuse reflectance spectroscopy for the diagnosis of breast cancer," *IEEE Trans. Biomed. Eng.* **50**, 1233–1242 (2003).

26. D. L. Heintzelman, U. Utzinger, H. Fuchs, A. Zuluga, K. Gossage, A. M. Gillenwater, R. Jacob, B. Kemp, and R. Richards-Kortum, "Optimal excitation wavelengths for in vivo detection of oral neoplasia using fluorescence spectroscopy," *Photochem. Photobiol.* **72**, 103–

113 (2000).

27. L. Coghlan, U. Utzinger, R. Drezek, D. Heintzelman, A. Zuluga, C. Brookner, R. Richards-Kortum, I. Gimenez-Conti, and M. Follen, "Optimal fluorescence excitation wavelength for detection of squamous intra-epithelial neoplasia: results from an animal model," *Opt. Express* **7**, 436–446 (2000).

28. W. Zeng, W. Lau, C. Cheng, K. C. Soo, and M. Olivo, "Optimal excitation-emission wavelengths for autofluorescence diagnosis of bladder tumors," *Int. J. Cancer* **104**, 477–481 (2003).

29. T. Vo-Dinh, "Multicomponent analysis by synchronous luminescence spectrometry," *Anal. Chem.* **50**, 396–401 (1978).

30. T. Vo-Dinh, "Synchronous luminescence spectroscopy: methodology and applicability," *Appl. Spectrosc.* **36**, 576–581 (1982).

31. C. L. Stevenson and T. Vo-Dinh, "Laser-excited synchronous luminescence spectroscopy," *Appl. Spectrosc.* **47**, 430–435 (1993).

32. W. E. Watts, N. R. Isola, D. Frazier, and T. Vo-Dinh, "Differentiation of normal and neoplastic cells by synchronous fluorescence: rat liver epithelial and rat hepatoma cell models," *Anal. Lett.* **32**, 2583–2594 (1999).

33. T. Vo-Dinh, "Principles of synchronous luminescence technique for biomedical diagnostics," *Proc. SPIE* **3911**, 42–49 (2000).

34. S. K. Majumdar and P. K. Gupta, "Synchronous luminescence spectroscopy for oral cancer diagnosis," *Lasers Life Sci.* **9**, 143–152 (2000).

35. T. J. Slaga, "Mechanisms involved in two-stage caracinogenesis in mouse skin," in *Mechanisms of Tumor Progression*, Vol. II, T. J. Slaga, Ed., pp. 1–15, CRC Press, Boca Raton, FL (1984).

36. StatSoft, Inc., *Electronic Statistics Textbook*, StatSoft, Tulsa, OK (2004); http://www.statsoft.com/textbook/stathome.html.

37. N. Ramanujam, M. F. Mitchell, A. Mahadevan, S. Thomsen, A. Malpica, T. Wright, N. Atkinson, and R. Richards-Kortum, "Development of a multivariate statistical algorithm to analyze human vervical tissue fluorescence spectra acquired in *vivo*," *Lasers Surg. Med.* **19**, 46–62 (1996).

38. S. Madhuri, N. Vengadesan, P. Aruna, D. Koteeswaran, P. Venkatesan, and S. Ganesan, "Native fluorescence spectroscopy of blood plasma in the characterization of oral malignancy," *Photochem. Photobiol.* **78**, 197–204 (2003).

39. P. E. Green, *Analyzing Multivariate Data*, Dryden Press, Hinsdale, IL (1978).

40. D. J. Hand, *Discrimination and Classification*, in Wiley series in probability and mathematical statistics, D. J. Hand, Ed., John Wiley & Sons, New York (1981).

41. T. Hastie, R. Tibshirani, and J. Friedman, "Model assessment and selection," in *The Elements of Statistical Learning*, T. Hastie, R. Tibshirani, and J. Friedman, Eds., pp. 193–224, Springer, New York (2001).

42. B. Efron, "Estimating the error rate of a prediction rule: some improvements on cross-validation," *J. Am. Stat. Assoc.* **78**, 316–331 (1983).

43. G. A. Wagnieres, W. M. Star, and B. C. Wilson, "In vivo fluorescence spectroscopy and imaging for oncological applications," *Photochem. Photobiol.* **68**, 603–632 (1998).

44. J. Sandby-Møller, T. Poulsen, and H. C. Wulf, "Influence of epidermal thickness, pigmentation and redness on skin autofluorescence," *Photochem. Photobiol.* **77**, 616–620 (2003).

45. I. Georgakoudi, B. C. Jacobson, M. G. Muller, E. E. Sheets, K. Badizadegan, D. L. Carr-Locke, C. P. Crum, C. W. Bonne, R. R. Dasari, J. Van Dam, and M. S. Feld, "NAD(P)H and collagen as in vivo quantitative fluorescent biomarker of epithelial precancerous changes," *Cancer Res.* **62**, 682–687 (2002).

46. B. K. Manjunath, J. Kurein, L. Rao, C. Muralikrishna, M. S. Chidananda, K. Venkatakrishna, and V. B. Kartha, "Autofluorescence of oral tissue for optical pathology in oral malignancy," *J. Photochem. Photobiol., B* **73**, 49–58 (2004).

47. C. Remington, "Porphyrin and haem biosynthesis and its control," *Acta Med. Scand.* **179**, 11–24 (1966).

48. J. Marriott, "Regulation of porphyrin synthesis," *Biochem. Soc. Symp.* **28**, 61–74 (1968).

49. L. Coghlan, U. Utzinger, R. Richards-Kortum, C. Brookner, A. Zuluaga, I. Gimenez-Conti, and M. Follen, "Fluorescence spectroscopy of epithelial tissue through the dysplasia-carcinoma sequence in an animal model: spectroscopic changes precede morphologic changes," *Lasers Surg. Med.* **29**, 1–10 (2001).